Bioactive Materials 6 (2021) 941–950

Contents lists available at ScienceDirect

Bioactive Materials

journal homepage: http://www.keaipublishing.com/biomat

Overcoming bacterial physical defenses with molecule-like ultrasmall antimicrobial gold nanoclusters

Kaiyuan Zheng[a], Magdiel I. Setyawati[b], David Tai Leong[a,*], Jianping Xie[a,**]

[a] Department of Chemical and Biomolecular Engineering, National University of Singapore, 4 Engineering Drive 4, 117585, Singapore
[b] School of Materials Science and Engineering, Nanyang Technological University, 50 Nanyang Avenue, 639798, Singapore

ARTICLE INFO

Keywords:
Gold nanoclusters
Gold nanoparticles
Antimicrobial agents
Molecule-like properties
Size effects

ABSTRACT

The size of metal nanoparticles (NPs) is crucial in their biomedical applications. Although abundant studies on the size effects of metal NPs in the range of 2–100 nm have been conducted, the exploration of the ultrasmall metal nanoclusters (NCs) of ~1 nm in size with unique features is quite limited. We synthesize three different sized gold (Au) NCs of different Au atom numbers and two bigger sized Au NPs protected by the same ligand to study the size influence on antimicrobial efficacy. The ultrasmall Au NCs can easily traverse the cell wall pores to be internalized inside bacteria, inducing reactive oxygen species generation to oxidize bacterial membrane and disturb bacterial metabolism. This explains why the Au NCs are antimicrobial while the Au NPs are non-antimicrobial, suggesting the key role of size in antimicrobial ability. Moreover, in contrast to the widely known size-dependent antimicrobial properties, the Au NCs of different atom numbers demonstrate molecule-like instead of size-dependent antimicrobial behavior with comparable effectiveness, indicating the unique molecule-like feature of ultrasmall Au NCs. Overcoming the bacterial defenses at the wall with ultrasmall Au NCs changes what was previously believed to harmless to the bacteria instead to a highly potent agent against the bacteria.

1. Introduction

Physicochemical properties of nanomaterials can greatly influence their biological behaviors and biomedical applications [1–5]. Chief among them is the size of nanomaterials, which will determine the intracellular uptake, transport and accumulation, their resultant efficacies as anti-cancer and anti-bacterial agents, and ultimately their *in vivo* bio-distribution and clearance [6–8]. Also, stability of nanomaterials is an important factor, the aggregation or degradation will influence their individual size and surface area, leading to huge influence towards biomedical applications [9–11]. While, size influences on properties of nanoparticles (NPs)' in the range of 2–100 nm is an acceptable phenomenon, mechanistic studies are unable to be done on large sized NPs as differences in atom numbers per particle do not induce a significant change in their properties. However, when we decrease the sizes of metal particles to less than 300 metal atoms (~1 nm in size), every single atom change makes a discernible change. Ultrasmall metal NPs, called metal nanoclusters (NCs), are discrete entities with defined atom numbers to an extent that they are better defined as "molecule-like" than "particle-like". The metal NCs possess well-defined molecular formulae and structures, quantized charging, highest occupied molecular orbital-lowest unoccupied molecular orbital (HOMO-LUMO) transitions, molecular magnetism, molecular chirality, and strong luminescence, which are not presented in bigger sized metal NPs system [12–24]. Moreover, their unique properties lead to particular biomedical applications in bioimaging, biosensing, biocatalysis, cancer therapy, drug delivery, *etc*. [25–32] The metal NCs are important tools for impactful biomedical mechanistic understanding on the physics and chemistry interactions and contributions to their physicochemical properties at the atomically precise level.

Recently, we found that ultrasmall gold (Au) NCs are antimicrobial, while their larger counterparts Au NPs of 6 nm protected by the same ligand are non-antimicrobial [33]. There are also other reports on the antimicrobial ability of Au NCs [34–36]. Similarly, it is reported that Au NCs showed efficient catalytic activity for selective oxidation, while slightly larger Au NPs were completely inactive [37]. Another example is that Au NCs showed strong toxicity towards various human cancer cells, but Au NPs were non-toxic [38]. These studies highlight the fundamental differences of Au NCs from Au NPs in their biological behaviors and biomedical applications, indicating the necessity of

Peer review under responsibility of KeAi Communications Co., Ltd.
* Corresponding author.
** Corresponding author.
E-mail addresses: cheltwd@nus.edu.sg (D.T. Leong), chexiej@nus.edu.sg (J. Xie).

https://doi.org/10.1016/j.bioactmat.2020.09.026
Received 19 August 2020; Received in revised form 24 September 2020; Accepted 27 September 2020
2452-199X/ © 2020 The Authors. Publishing services by Elsevier B.V. on behalf of KeAi Communications Co., Ltd. This is an open access article under the CC BY-NC-ND license (http://creativecommons.org/licenses/BY-NC-ND/4.0/).

thorough investigation on the ultrasmall Au NCs rather than simply extrapolating the knowledge derived from the Au NPs studies.

In contrast to the bigger sized metal NPs, the atom number inside each metal NC would greatly influence corresponding properties and applications, in which two NCs with only a few atoms difference could induce huge effect or even contrasting biological behaviors. For example, Au_{15} NCs showed the competitive Langmuir-Hinshelwood catalytic mechanism with a strong substrate binding and weak product binding ability. In contrast, larger Au_{18} and Au_{25} NCs (only 3 and 10 Au atoms difference) demonstrated similar catalytic performance as Au NPs, which were attributed to the non-competitive Langmuir-Hinshelwood mechanism with a weak substrate binding and strong product binding ability [39]. In another study, smaller Au NCs (*i.e.*, $Au_{10\text{-}11}$, Au_{15}, and Au_{18}) showed significantly reduced renal clearance efficiency (4–9 times) compared to the slightly larger Au_{25} NCs, which could be attributed to the more readily trapped of smaller Au NCs by the glomerular glycocalyx [29]. Such sensitive physique makes Au NCs as a great platform to understand the size effect towards various properties and applications at atomically precise level.

Although we have reported the unexpected antimicrobial ability of Au NCs which was absent for Au NPs, the underlying reason of the Au NPs' non-existence antimicrobial activity as well as the influence of the Au NCs size (*i.e.* atom number per NC) towards their antimicrobial efficacy are yet unknown [33]. Therefore, in the current work, we have moved one step further to use three different sized ultrasmall Au NCs (Au_{25}, Au_{102}, and Au_{144}) and two larger sized Au NPs (~3 and 5 nm) protected by the same ligand to study their bacterial killing behaviors. Comparison of Au NCs and Au NPs internalization by the bacteria showed crucial internalization "size cutoff" that determines their antimicrobial ability. The ultrasmall Au NCs were effectively internalized by the bacteria to achieve high antimicrobial activity, while larger sized Au NPs were poorly internalized and failed to show any antimicrobial performance. Overcoming the bacterial defenses at the wall with ultrasmall Au NCs changes what was previously believed to harmless to the bacteria instead to a highly potent agent against the bacteria. Moreover, in contrast to the previous size-dependent studies, the three Au NCs showed molecule-like instead of size-dependent antimicrobial ability in comparable effectiveness, suggesting the Au NCs work as an active molecule to kill bacteria. Thereafter, the internalized Au NCs induce reactive oxygen species (ROS) generation to oxidize bacterial membrane and perturb bacterial metabolism, leading to eventual bacterial killing from the inside instead of the less effective dilutive outside-in strategies deployed by other much larger antimicrobial nanomaterials. While size matters is a "back-of-the-mind" parameter to many researchers working on antimicrobial agents, here we argued and showed that revisiting size and downsizing the nanomaterials can have a profound effect on delivering agents into target cells with high efficacious outcomes in biomedical applications; thus shedding light on the rational design of new antimicrobial agents and other theranostic probes through atomically precise manipulation of size.

2. Experimental section

2.1. Materials

Ultrapure water (18.2 MΩ) was used throughout the study. All glassware and magnetic stir bars were washed with *aqua regia*, rinsed with abundant ethanol and ultrapure water, and dried in an oven before use. All chemicals were commercially available and used as received: gold (III) chloride trihydrate ($HAuCl_4{\cdot}3H_2O$), *p*-mercaptobenzoic acid (MBA), sodium borohydride ($NaBH_4$), ammonium acetate (NH_4OAc), agar, lysozyme, lysostaphin, 2′,7′-dichlorofluorescein diacetate (DCFH-DA), paraformaldehyde (PFA), and 2,5-dihydroxybenzoic acid (DHB) were purchased from Sigma-Aldrich; sodium hydroxide (NaOH) was from Merck; Luria − Bertani (LB) was from Becton Dickinson; Hoechst 33342, SYTOX® Green nucleic acid stain and ProLong® Gold antifade reagent with DAPI were purchased from Life Technologies; lipid peroxidation (MDA) assay kit was purchased from Abcam.

2.2. Instruments

UV–vis absorption spectra of the samples were recorded by a Shimadzu UV-1800 photospectrometer. Transmission electron microscopy (TEM) images were taken on a JEOL JEM 2010 microscope operating at 200 kV. Zeta potential was measured on Malvern DLS (Dynamic light scattering). Inductively coupled plasma optical emission spectrometry (ICP-OES) was used to determine the concentration of Au atoms in solution, which was measured through iCAP 6000 Series, Thermo Scientific. The molecular weight of Au NCs was obtained by electrospray ionization (ESI) mass spectrometry on a Bruker microTOF-Q system, and matrix-assisted laser desorption ionization-time-of-flight (MALDI-TOF) mass spectrometer on a Bruker Daltonics Autoflex II TOF/TOF system. Optical density at 600 nm (OD_{600}) of bacterial cells and fluorescence intensity of dyes were measured on microplate reader Biotek H4FM. The bacteria fluorescent images were taken with an epifluorescence microscope Leica DMI6000.

2.3. Synthesis of Au_{25} NCs

The synthesis of Au_{25} NCs was according to a reported method [40]. First, freshly prepared aqueous solutions of $HAuCl_4$ (40 mM, 0.25 mL) and MBA (50 mM in 0.15 M NaOH, 0.4 mL) were mixed in water (9.5 mL) under mild stirring, and light-yellow Au(I) − MBA complexes were formed for 2 h. Next, the pH of the solution was brought to 11.6 by using 1 M NaOH solution. Afterwards, CO was bubbled into the solution for 2 min. Then, the bottle was sealed airtight, and the product was collected after 72 h. Finally, a stirred ultrafiltration cell (Model 8010, Millipore Corporation, USA) with a semipermeable membrane of 3000 Da molecular weight cutoff (MWCO) was used to purify the sample, the purification time is ~1 h.

2.4. Synthesis of Au_{102} NCs

The synthesis of Au_{102} NCs was according to a reported method [41]. 0.209 g $HAuCl_4{\cdot}3H_2O$ was dissolved in 19 mL of water (0.028 M based on Au), and 0.292 g MBA was dissolved in 19 mL of 0.3 M NaOH solution (0.1 M based on MBA). First, 51.5 mL of water and 17.8 mL of the as-prepared $HAuCl_4$ solution were added in a 1 L flask. Next, 15.5 mL of the as-prepared MBA solution was immediately added, and the reaction solution turned from yellow to orange. Then, 75 mL of methanol was immediately added. The reaction was conducted under stirring at room temperature for 1 h, and the reaction solution turned from dark orange to light orange during this time. Afterwards, 20.8 mg $NaBH_4$ was added into the solution under stirring, and the reduction reaction was processed under stirring at room temperature for 17 h. The reaction solution turned black during this step. When the reaction finished, methanol was added into the flask until a total volume reached 800 mL, and NH_4OAc solution (5 M, 40 mL) was added. The reaction solution was then divided into twenty 50 mL centrifuge tubes, and centrifuged at 4000 rpm at 4 °C for 10 min. The precipitate was dried by inverting the tubes on paper towel for more than 1 h. Afterwards, the dry precipitate was dissolved in 0.2 mL of water, and the solutions were combined into 4 tubes. Then, NH_4OAc solution (2 M, 0.5 mL) was added into each tube, and methanol was added until the total volume reached 45 mL. The solution was mixed on the vortex, and then centrifuged at 4000 rpm at 4 °C for 10 min. Finally, the precipitate was dried in dry box for more than 2 h, and dissolved in water to obtain pure Au_{102} NCs.

2.5. Synthesis of Au_{144} NCs

The synthesis of Au_{144} NCs was according to a reported method

[41]. The first day, 95.2 mM MBA in NaOH solution (0.3 M) was prepared and shaked overnight. The second day, 28 mM $HAuCl_4$ soluiton was prepared, and then the Au(I)-MBA complex was generated by mixing the $HAuCl_4$ soluiton with the as-prepared MBA solution in the mixed solvent. In the final solution of mixed solvent (48 mL, 47% methanol and 53% water), MBA was 9 mM and $HAuCl_4$ was 3 mM. The complex solution was shaked overnight, which was clear and faint yellow. The third day, freshly prepared $NaBH_4$ solution (0.15 M, 0.48 mL) was added into the complex solution, followed by an immediate shaking for 2 h. Then, the reaction solution was centrifuged at 4000 rpm for 5 min. The precipitate was dissolved in 10 mL of water, and then precipitated again by adding NH_4OAc solution (2 M, 1 mL) and 20 mL of methanol, followed by centrifuging at 4000 rpm for 5 min. The washing process was repeated again, and the precipitate was resuspended in water to obtain pure Au_{144} NCs.

2.6. Synthesis of Au NPs

In a typical synthesis, freshly prepared aqueous solutions of $HAuCl_4$ (40 mM, 0.25 mL) and MBA (50 mM in 0.15 M NaOH, 1 mL) were mixed in water (8.75 mL) under mild stirring to generate Au NPs-3nm; $HAuCl_4$ (40 mM, 0.25 mL) and MBA (50 mM in 0.15 M NaOH, 0.067 mL) were mixed in water (9.7 mL) under mild stirring for producing of Au NPs-5nm. Next, the pH of the solution was brought to ~12 by using 1 M NaOH solution. After 1 h, freshly prepared $NaBH_4$ solution (112 mM in 0.2 M NaOH solution, 0.1 mL) was added into the reaction solution. The products were collected after 1 day, and ethanol was used to wash the Au NPs in solution after synthesis.

3. Results and discussions

In this study, we synthesized three different sized Au NCs and two different sized Au NPs with the same protecting ligand, *p*-mercaptobenzoic acid (MBA). As size is the central hypothesis of this study, synthesizing the Au particles with same protecting ligand is necessary to eliminate other factors that could influence the Au NCs antimicrobial performance, such as the surface charge effect [42]. As expected, the five Au particles protected by the same ligand hold similar electronegativity, as evidenced from their similar zeta potentials in the range of −32 to −38 mV. This confirms that we have successfully eliminated the surface charge effect, leaving the particle size as the only variable across the five Au particles to be tested in the following comparative antimicrobial studies.

The characterizations of the as-synthesized Au NCs and Au NPs are presented in Fig. 1. The first indication of their size difference could be observed from the color of the solutions (insets of Fig. 1a, c, e, g, i), where the Au NCs were noted to be yellowish to brownish in color, while Au NPs were reddish in color. The different color of the solutions is caused by the intrinsic electronic distinction between Au NCs and Au NPs. The bigger sized plasmonic Au NPs exhibited the well-known surface plasmon resonance (SPR) peak at ~520 nm (Fig. 1g,i), which presented red color solutions [44,45]. In contrast, reducing the particle size to Au NCs (< 2 nm) region led to strong quantum size effect, resulting in the disappearance of the SPR peaks (Fig. 1a,c,e). Thus, the Au NCs have discrete electronic states rather than continuous bands in metallic state, which can be clearly observed from their UV–vis absorption spectra [12]. As shown in Fig. 1a, Au_{25} NCs exhibited a main absorption peak at ~670 nm with two shoulder peaks at ~780 and ~400 nm, which are in good accordance with the reported characteristic absorption of Au_{25} NCs [46]. More importantly, the SPR peak at ~520 nm could not be detected, suggesting the as-synthesized products are not the bigger sized Au NPs, or contaminated with any Au NPs. Similarly, a featureless UV–vis absorption spectrum was observed for the Au_{102} NCs (Fig. 1c), while the absorption bands at 510 and 700 nm were detected for the case of Au_{144} NCs (Fig. 1e). Both of the UV–vis absorption characteristics are in good agreement with the previous reported results, confirming the successful synthesis of these Au NCs [47,48].

In addition, we used electrospray ionization mass spectrometry (ESI-MS) and matrix-assisted laser desorption ionization-time-of-flight mass spectrometry (MALDI-TOF-MS) to confirm the molecular formula of the as-synthesized Au NCs. As shown in the top panel of Fig. S1, two sets of peaks at *m/z* 1279 and 1540 were observed in the broad spectrum, which are $[Au_{25}MBA_{18} - 5H]^{6-}$ and $[Au_{25}MBA_{18} - 5H + Na]^{5-}$, respectively. As for the zoom-in spectrum, the peak at *m/z* 1540 corresponds to $[Au_{25}MBA_{18} - 5H + Na]^{5-}$, and the other peaks (2–14) are from the successive coordination of [+ Na–H] of peak 1. This verifies the high purity of the final product $Au_{25}MBA_{18}$. Moreover, as shown in Figs. S2 and S3, the single peak at *m/z* ~26820 and ~37540 represents $Au_{102}MBA_{44}$ and $Au_{144}MBA_{60}$, respectively. Moreover, the size of as-synthesized Au NCs and Au NPs was further characterized by transmission electron microscopy (TEM). As shown in Fig. 1b, d, f, the three Au NCs were found to have size less than 2 nm. As for the particle size distribution of Au NPs (inset of Fig. 1h, j), they were 3.0 ± 1.0 nm and 5.0 ± 2.0 nm, respectively. In addition, the Au NPs-3 nm and Au NPs-5 nm were estimated (see the Notes in Supporting Information) to have ~834 and ~3862 Au atoms, respectively. This agrees well with a previous report, which estimated the size of Au_{807} and Au_{4033} to be ~2.9 and 4.9 nm, respectively [49].

To explore the influence of particle size towards antimicrobial ability, we applied the as-synthesized series of three different sized Au NCs (*i.e.*, Au_{25}, Au_{102}, and Au_{144}) and two different sized Au NPs (*i.e.*, ~3 and ~5 nm) to observe their antimicrobial behavior. We first exposed the gram-positive bacteria *Staphylococcus aureus* (*S. aureus*) to the five Au particles of same Au atom concentration (0.1 mM on the basis of Au atoms in the treatment solution, which equals to $\sim 2.4 \times 10^{15}$ particle·mL^{-1} of Au_{25} NCs, $\sim 5.8 \times 10^{14}$ particle·mL^{-1} of Au_{102} NCs, $\sim 4.14 \times 10^{14}$ particle·mL^{-1} of Au_{144} NCs, $\sim 7.2 \times 10^{13}$ particle·mL^{-1} of AuNPs-3 nm, and $\sim 1.56 \times 10^{13}$ particle·mL^{-1} of AuNPs-5 nm; see Supporting Information for the calculation details). Consistent with our previous report, Au_{25} NCs showed the highest antimicrobial efficacy (~96%), while two Au NPs failed to exhibit any killing effect to the bacteria (Fig. 2a and b) [33]. However, we found that the antimicrobial performance of Au NCs was inversely correlated to the atom number per NC, in which Au_{102} and Au_{144} NCs only achieved ~35% and ~30% bacterial killing efficacy, respectively. The low bacterial killing efficacy given the fast nature of microbial growth will be counterproductive as the majority of the bacterial population remains highly viable and virulent. Time-dependent antimicrobial treatment also showed the gradually decreasing bacterial killing efficacy of Au_{102} and Au_{144} NCs as compared to Au_{25} NCs (Fig. 2c). It is worth noting that within this treatment condition, Au_{102} and Au_{144} NCs were both introduced at significantly lower particle concentration as compared to the high performing antimicrobial Au_{25} NCs, suggesting that the antimicrobial effect of these Au NCs might be correlated with their particle concentration rather than the atom concentration. Thus, we need to introduce fair amount of particle concentration to test their antimicrobial efficacy.

Therefore, we treated the bacteria with the as-synthesized five Au particles of the same particle concentration rather than the same Au atom concentration (*i.e.*, $\sim 2.4 \times 10^{15}$ particle·mL^{-1}, the detailed treatment concentration of each group could be found in Supporting Information). In contrast to the reported size-dependent catalytic and renal clearance behaviors, all three Au NCs showed similar high antimicrobial efficacy of > 96% (Fig. 3a and b), indicating that their antimicrobial ability was independent of their size (Au atom number per NC) [29,39]. Moreover, their time-dependent bacterial killing curves were of the same trend (Fig. 3c), further suggesting their comparable antimicrobial behaviors. However, we observed perceivable decrease in bacterial killing effect over time, which was presumably caused by insufficient supply of Au NCs to eradicate all bacteria in the system. Increasing the concentration of Au NCs to 5-fold (*i.e.*, $\sim 1.2 \times 10^{16}$

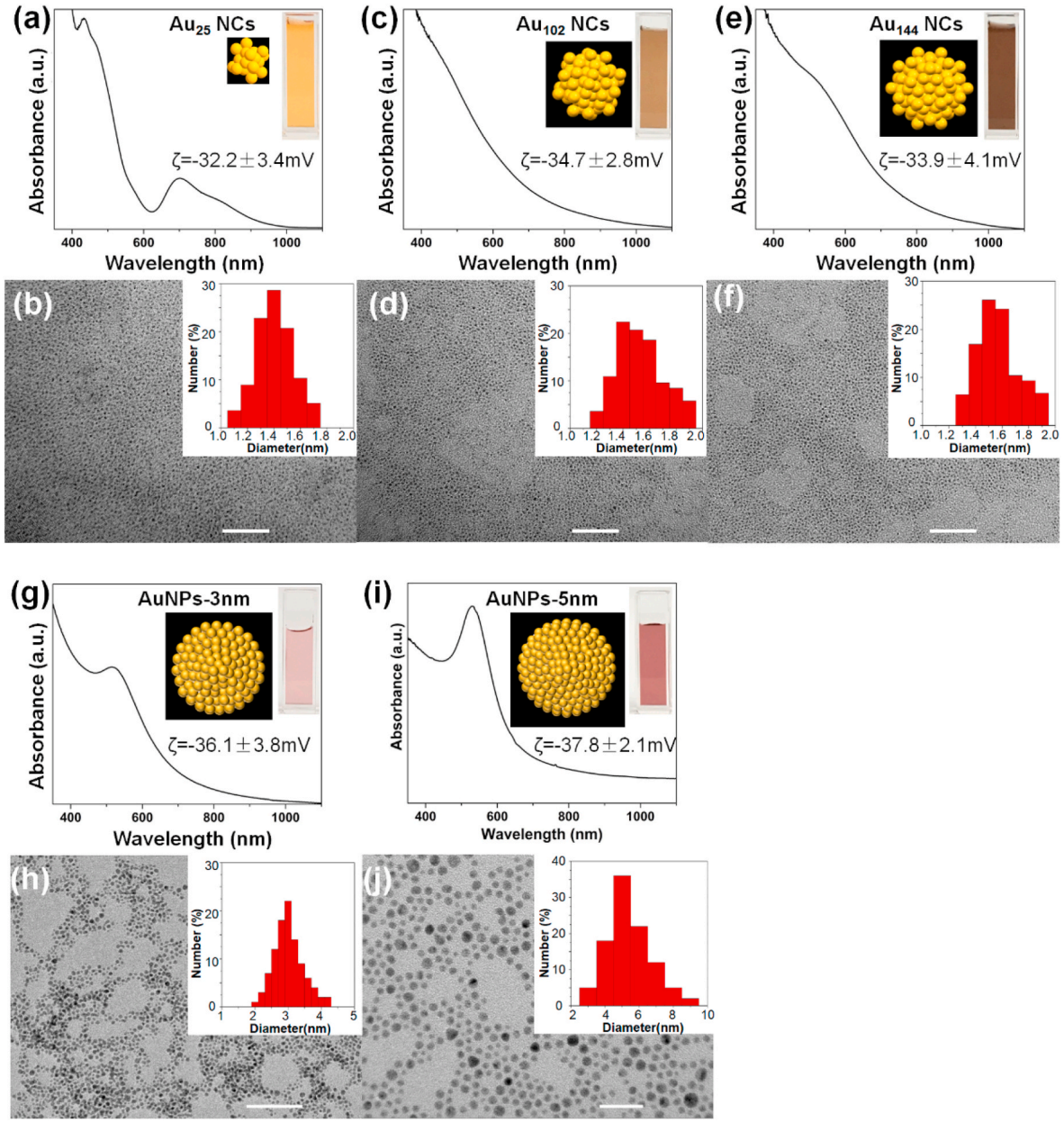

Fig. 1. Characterization of as-synthesized Au NCs and Au NPs. (a, c, e, g, i) UV–vis absorption spectra of MBA-protected Au_{25} NCs, Au_{102} NCs, Au_{144} NCs, Au NPs-3 nm, and Au NPs-5 nm. The insets are corresponding digital photos of the NC or NP solutions, their crystal structures and zeta potentials (ζ) [43]. (b, d, f, h, j) Representative TEM images. The insets are the size distribution of the corresponding NCs or NPs. The scale bar is 20 nm.

particle·mL^{-1}) allowed the three Au NCs to maintain their high antimicrobial efficacy (> 96% cell death) following a prolonged treatment of 24 h (Fig. S4). In addition, we measured IC_{50} values of the three Au NCs, which are all ~2.4 μM on the basis of Au NCs concentration that equals to ~1.4 × 10^{15} particle·mL^{-1} (Fig. 3d). Furthermore, our control groups showed negligible antimicrobial killing effect on bacterial cells treated with MBA ligands, Au(I)-MBA complexes and Au ions (Fig. S5), suggesting only intact Au NCs in their entities could exert antimicrobial effect. Overall, these results strongly support our hypothesis that the Au NCs enact their antimicrobial properties in a molecule-like manner rather than in a size-dependent manner, and their killing efficacy strongly correlates with the active molecular number of Au NCs in the treatment solution.

Notably, neither of the Au NPs exhibited any bacterial killing ability (Fig. 3a and b). We measured the uptake of Au particles inside the bacteria and found that significantly lower amount of Au NPs were internalized by the bacterial cells (Fig. 3e). Estimation based on the Au atoms concentration showed higher uptake of Au NPs as compared to Au NCs (Fig. S6). However, converting this atom concentration through atom number/particle correlation provides us with the true amount of the internalized particle numbers (Fig. 3e). The uptake of Au NCs inside the bacteria was about ~1 × 10^{14} Au particle/mg DWC (dry weight of the cell pellet), while Au NPs-3 nm and Au NPs-5 nm were determined to be ~2.6 × 10^{13} and 3.6 × 10^{12} (~26% and 3.3% of Au NCs), respectively. Such low internalization of Au NPs supports our hypothesis that the lack of antimicrobial properties of Au NPs possibly stem from their poor cellular uptake.

In between, we used another comparator sample, $Au_{\sim 250}MBA_n$ NCs with diameter of ~2 nm, to test their antimicrobial ability [50]. The UV–vis spectrum and TEM image of the as-synthesized $Au_{\sim 250}MBA_n$ NCs were presented in Figs. S7a and S7b, which match well with the previous report [50], suggesting the successful synthesis of the final

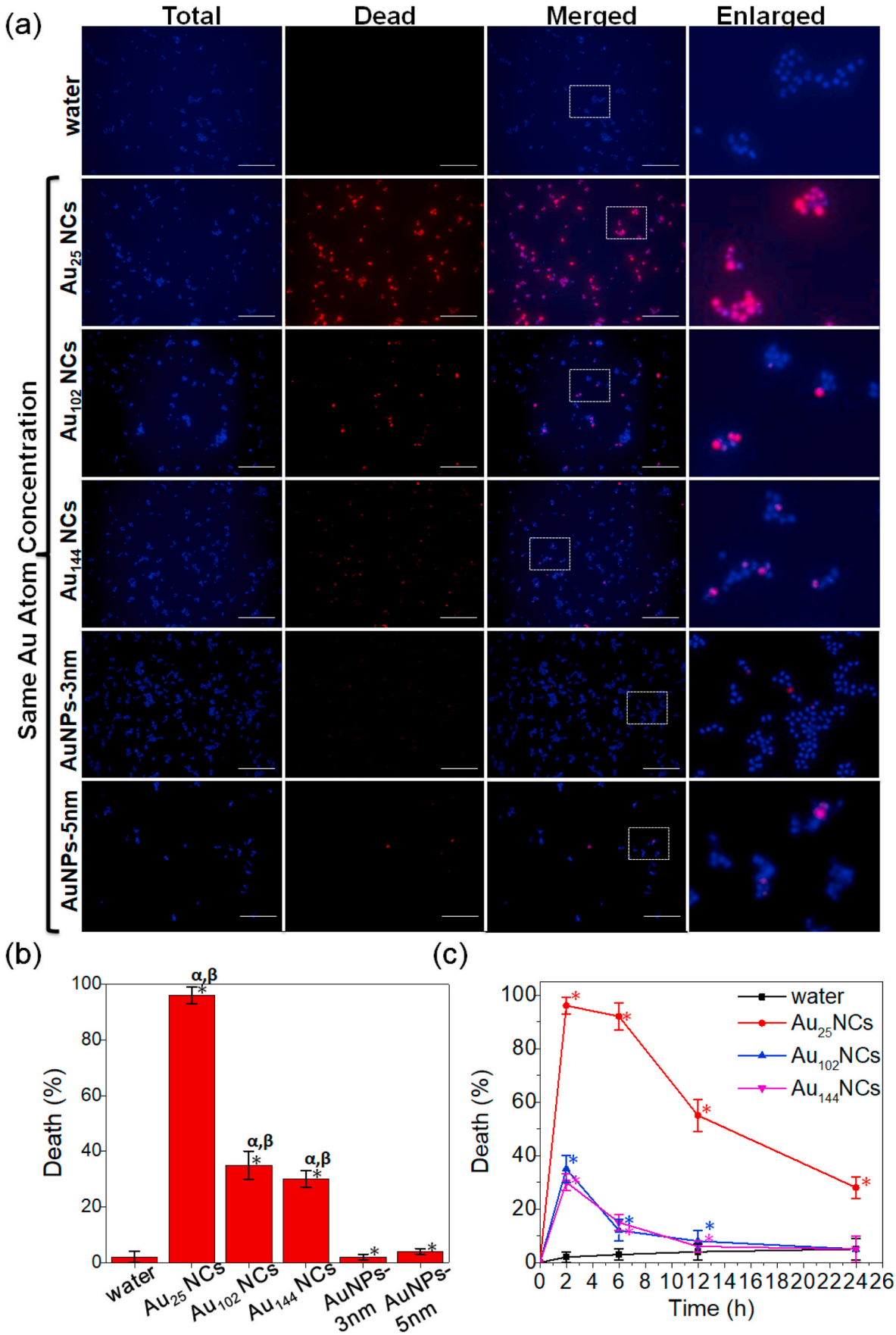

(caption on next page)

Fig. 2. Au NCs showed different antimicrobial ability under the same Au atom concentration, and Au NPs did not show antimicrobial ability. (a) Representative fluorescence images of the *S. aureus* after 2 h treatment of Au NCs and Au NPs at the same Au atom concentration (the final Au atom concentration in the treatment solution was 0.1 mM). The dead cells were stained by SYTOX green (pseudo color: red), while total cells were stained by Hoechst 33342 (blue). Scale bar is 25 μm. (b) Percentage of the dead *S. aureus* treated with Au NCs and Au NPs at the same Au atom concentration for 2 h. Data are means ± S.D., n = 3, Student's *t*-test; * significant against the water-treated group, $p < 0.05$; $^{\alpha}$ significant against the Au NPs-3 nm treated group, $p < 0.05$; $^{\beta}$ significant against the Au NPs-5 nm treated group, $p < 0.05$. (c) Time-dependent curve of percentage of dead *S. aureus* after being treated with Au NCs at the same Au atom concentration for 2, 6, 12 and 24 h. Data are means ± S.D., n = 3, Student's *t*-test; * significant against the water-treated group, $p < 0.05$. (For interpretation of the references to color in this figure legend, the reader is referred to the Web version of this article.)

product. As for the size distribution, the particles ranged from 1.5 to 2.5 nm could be observed (inset of Fig. S7b). Notably, the as-synthesized product $Au_{\sim 250}$ is not a monodispersed single species Au_{250} as other three Au NCs (i.e., Au_{25}, Au_{102} and Au_{144}), and the Au atom number per particle is also estimated from the TEM images [50]. As shown in Figs. S7c and S7d, the $Au_{\sim 250}$-treated group could only achieve ~72% bacterial killing efficacy, which is lower than the > 96% antimicrobial effect of Au_{25}-treated group. Such decreased antimicrobial behavior could be caused by their lower uptake inside bacteria (Fig. S7e), for some bigger sized particles (> 2 nm) would not be effectively internalized by the bacteria, resulting in lower antimicrobial ability as compared to the other three variants of Au NCs. This could further support our conclusion that the uptake ability of particles inside bacteria determines their antimicrobial ability."

In addition, we treated gram-negative bacteria *Escherichia coli* (*E. coli*) with the three Au NCs and two Au NPs of the same particle concentration. Consistently, it was demonstrated that all three Au NCs exhibited comparable high antimicrobial ability, whereas the two Au NPs did not show obvious antimicrobial efficacy (Fig. S8a). Moreover, the uptake of Au NCs and Au NPs in the bacteria was also significantly different (Fig. S8b). The internalized Au NCs was about $\sim 0.7 \times 10^{14}$ Au particle/mg DWC, while Au NPs-3 nm and Au NPs-5 nm were only $\sim 1.4 \times 10^{13}$ and $\sim 4.9 \times 10^{12}$ (~20% and ~7% of Au NCs), respectively.

The contrasting internalization profile between the Au NPs and Au NCs clearly showed the fundamental role of nanomaterials' size in determining their biomedical applications. One deterministic feature of the bacterial membrane that could regulate nanomaterials uptake is the membrane pores, where the nanomaterials could simply diffuse into the bacteria. Pores, like those formed by porin trimers, typically are 1.2–2 nm in diameter [51], which could facilitate easy and rapid internalization of ultrasmall Au NCs (< 2 nm). Unlike mammalian and other eukaryotic cells, bacterial cells do not have the same active vesicular endocytosis machinery to internalize nanomaterials. Thus, the nanomaterials could only enter the bacterial cells through ultrasmall pores on the cell wall based on simple diffusion. This provides opportunities for the ultrasmall Au NCs to get effectively internalized by the bacteria to achieve high antimicrobial activity. In contrast, larger sized Au NPs are highly restricted to enter through these pores, resulting in their less efficient uptake into the bacterial cells. The "size cutoff" in internalization could be the reason for the contrasting antimicrobial behaviors of Au NCs and Au NPs. This also indicates the key role of nanomaterials uptake during biomedical applications, that sometimes the nanomaterials didn't achieve expected efficacy might simply be caused by the insufficient internalization.

Moreover, once the Au NCs have entered the bacteria, only the number of Au NCs being internalized would determine their antimicrobial ability, and the Au atom number per NC would not influence any killing effect exerted by the NCs. As a result, the Au NCs show molecule-like instead of size-dependent antimicrobial ability, which represents the status that Au NCs have been internalized inside bacteria. Since similar number of three Au NCs have been internalized (Fig. 3e and S8b), they showed similar antimicrobial ability (Fig. 3a–d, S8a), but their different size/atom number did not affect their antimicrobial ability. Another significant feature of Au NCs is their unique molecular structure, that each species hold specific morphology and molecular packing, which could not be found in spherical Au NPs [12]. The three Au NCs (i.e. Au_{25}, Au_{102}, and Au_{144}) used in this study hold different structures as reported (shown in insets of Fig. 1) [13,52,53]; however, they still showed similar antimicrobial ability. This suggests that the molecular structure or morphology of Au NCs would not influence their antimicrobial efficacy, which is also different from bulky NPs, further indicating the unique property of nanomaterials at ultrasmall NCs range. Thus, we describe this phenomenon as "molecular-like" antimicrobial ability, wherein each Au NC act like a molecule, regardless their size/atom number/structure.

We have reported that Au NCs could induce intracellular ROS generation to disrupt the normal bacterial metabolism, resulting in eventual cell death [33]. We further investigated the capability of Au NCs and Au NPs in inducing the intracellular ROS production. Consistent with the antimicrobial behavior (Fig. 3), all three Au NCs induced significant increase of the intracellular ROS production (~1.8–2.2-fold) in *S. aureus* after 2 h treatment, while two Au NPs exhibited appreciably lower ROS generation (~1.1–1.3-fold) as shown in Fig. 4a. Recently, we found that the Au NCs would become decomposed into smaller sized Au NCs, which would lose electrons to active oxygen. Thus, the oxygen would be activated by the electrons transferred from Au NCs, leading to the formation of superoxo and peroxo-like species, inducing ROS generation inside bacteria to achieve killing effect [54]. The different ROS producing behaviors between Au NCs and Au NPs could also be attributed to their different uptake ability, in which the ultrasmall Au NCs could be easily internalized to perturb the bacterial metabolic pathway and react with sub-cellular structures [33]. Moreover, no appreciable difference in ROS generation between the three Au NCs groups was observed. In particular, the Au_{25} NCs induced ~1.8-fold ROS generation, while Au_{102} and Au_{144} NCs caused slightly higher ROS production of ~2.1-fold and ~2.2-fold, respectively. This is consistent with the antimicrobial efficacy (Fig. 3a and b) and uptake ability (Fig. 3e) of these three Au NCs, which are also at a comparable level, further reinforcing that the Au NCs possess molecule-like instead of size-dependent antimicrobial behavior. In good agreement with the observation in *S. aureus* system, increasing ROS production in *E. coli* treated with the three Au NCs were found to be ~1.8–2.0-fold (Fig. S9). The production of ROS intracellularly is very important for the antimicrobial effect as extracellular ROS production is greatly dilutive by the extracellular environment. Even though other nanomaterials are known to be ROS productive [55–57,66], their application as antimicrobial agents become greatly limited by their inability to enter the bacterial cells.

Moreover, the ROS produced by Au NCs could also oxidize the bacterial membrane, exacerbating the bacterial membrane damage [58]. To verify the bacterial membrane damage caused by the generated ROS, we tested the lipid peroxidation of bacteria after treatment of Au NCs. Lipid peroxidation is the oxidative degradation of lipids to produce reactive aldehydes (*e.g.* malondialdehyde (MDA) and 4-hydroxynonenal (4- HNE)) as final products, which would react with thiobarbituric acid (TBA) to generate fluorescent MDA-TBA adducts for detection [59]. As shown in Fig. 4b, all Au NCs-treated groups resulted in significantly higher bacterial membrane lipid peroxidation as compared to the Au NPs-treated groups, indicating the generated ROS could oxidize the bacterial membrane lipid efficiently. Thereafter, larger holes would gradually be appearing on the bacterial membrane, leading

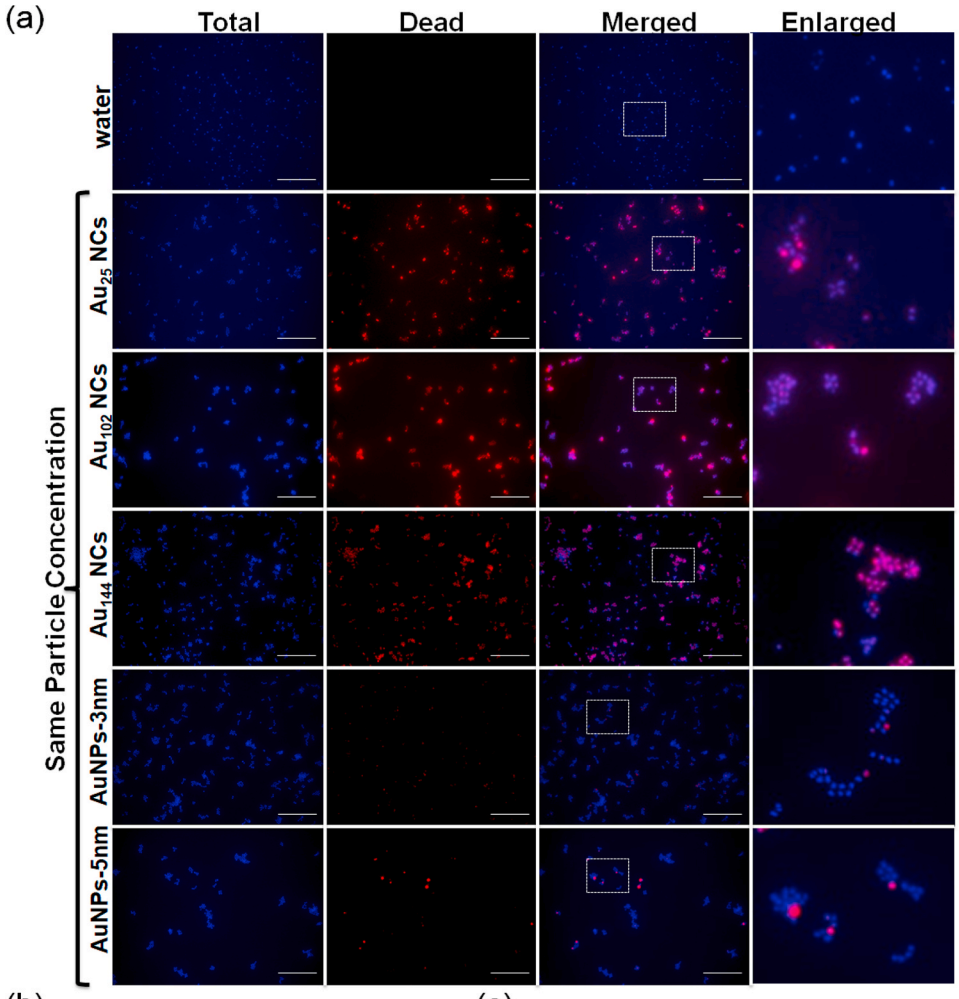

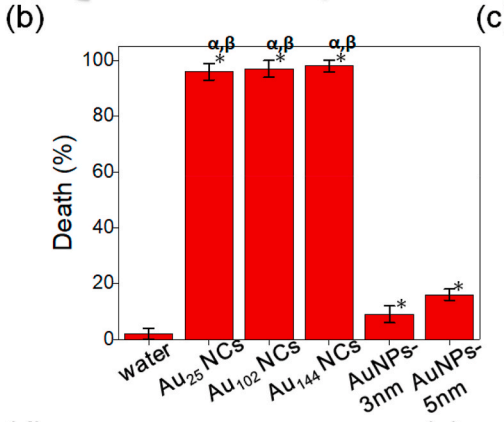

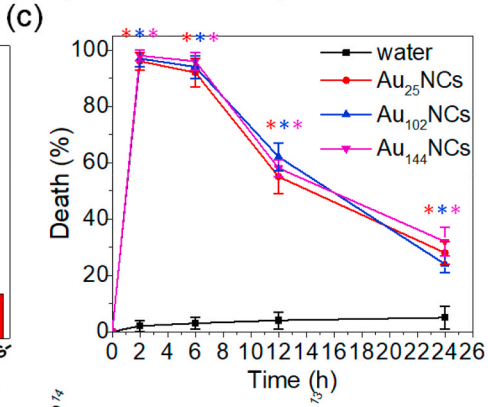

(d)

IC_{50}	Au atom [μM]	Au NCs [μM]
Au_{25}	61.2	2.4
Au_{102}	254.6	2.5
Au_{144}	331.1	2.3

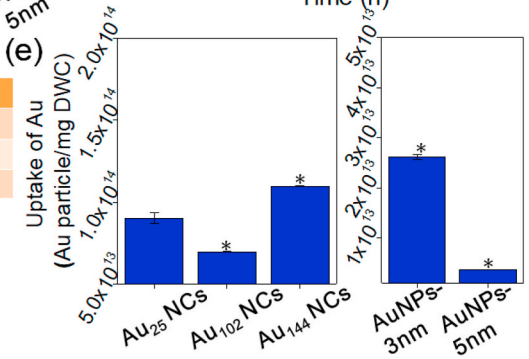

Fig. 3. Au NCs showed similar high bacterial internalization and antimicrobial ability under the same particle concentration, while Au NPs showed lower uptake in the bacteria and did not show obvious bacterial killing efficiency. (a) Representative fluorescence images of the *S. aureus* after 2 h treatment of Au NCs and Au NPs at the same particle concentration (the final particle concentration in the treatment solution was ~2.4×10^{15} particle·mL^{-1}). The dead cells were stained by SYTOX green (pseudo color: red), while total cells were stained by Hoechst 33342 (blue). Scale bar is 25 μm. (b) Percentage of the dead *S. aureus* treated with Au NCs and Au NPs at the same particle concentration for 2 h. Data are means ± S.D., n = 3, Student's *t*-test; * significant against the water-treated group, $p < 0.05$; $^{\alpha}$ significant against the Au NPs-3 nm treated group, $p < 0.05$; $^{\beta}$ significant against the Au NPs-5 nm treated group, $p < 0.05$. (c) Time-dependent curve of percentage of dead *S. aureus* after being treated with Au NCs at the same particle concentration for 2, 6, 12 and 24 h. Data are means ± S.D., n = 3, Student's *t*-test; * significant against the water-treated group, $p < 0.05$. (d) Half maximal inhibitory concentration (IC_{50}) of Au NCs towards *S. aureus*. (e) Uptake of Au NCs and Au NPs in *S. aureus* after 2 h treatment at the same particle concentration. Data are means ± S.D., n = 3, Student's *t*-test; * significant against the Au_{25} NCs-treated group, $p < 0.05$. (For interpretation of the references to color in this figure legend, the reader is referred to the Web version of this article.)

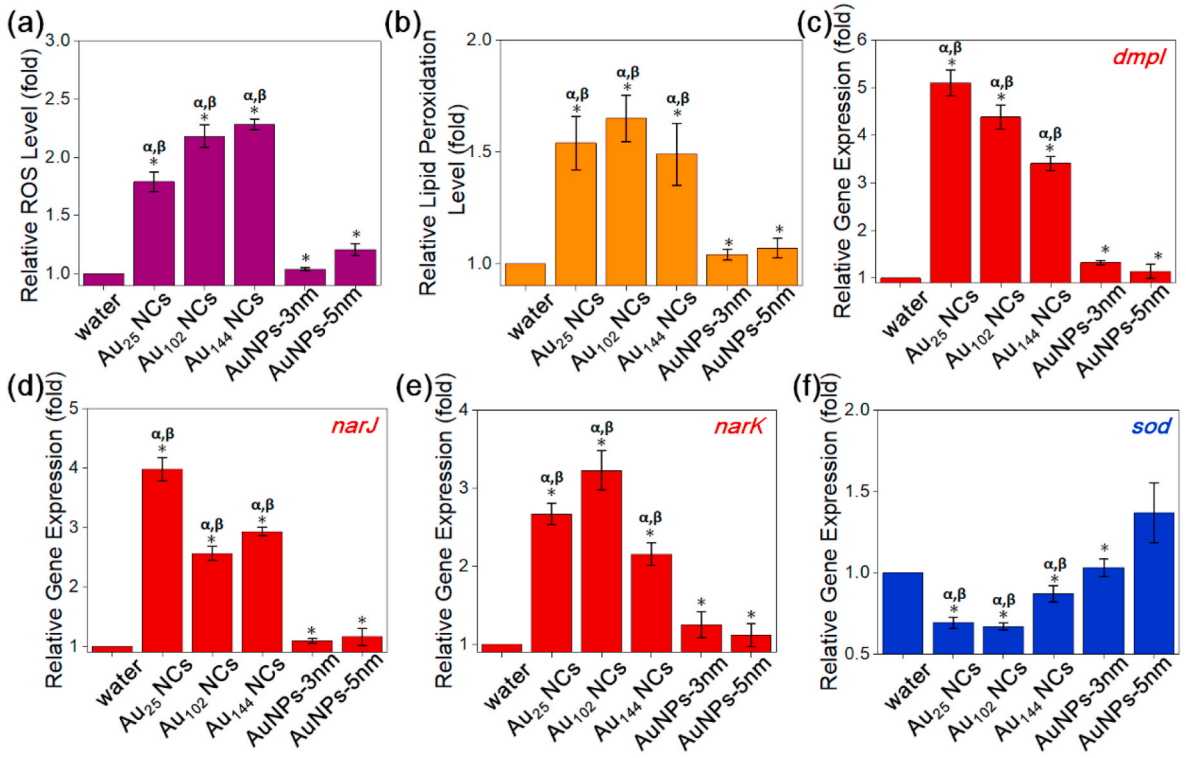

Fig. 4. Au NCs induced intracellular ROS generation, oxidized bacterial membrane and promoted cellular oxidation process in *S. aureus*. (a) Relative intracellular ROS production level and (b) relative lipid peroxidation production level of *S. aureus* after 2 h treatment of Au NCs and Au NPs at the same particle concentration (the final particle concentration in the treatment solution was ~2.4 × 10^{15} particle·mL^{-1}). The intracellular ROS level and the lipid peroxidation level of the water-treated group were set as 1. (c–f) Relative gene expression of *S. aureus* after 2 h treatment of Au NCs and Au NPs at the same particle concentration. The gene expression of the water-treated group was set as 1. Increased expression of the oxidation regulating gene (c) *dmpI*, (d) *narJ*, (e) *nark*, and decreased expression of the reduction regulation gene (f) *sod* were observed. Data are means ± S.D., n = 3, Student's *t*-test; * significant against the water-treated group, $p < 0.05$; $^{\alpha}$ significant against the Au NPs-3 nm treated group, $p < 0.05$; $^{\beta}$ significant against the Au NPs-5 nm treated group, $p < 0.05$.

to extensive bacterial membrane damage. This could also facilitate further internalization and accumulation of the Au NCs inside bacteria, resulting in the enhanced bacteria killing efficacy.

In addition, since ROS is the byproduct of intracellular redox metabolism, the different ROS production between Au NCs and Au NPs treated groups could be caused by the different bacterial redox response towards them [60,61]. We chose four indicator genes (*i.e.*, three oxidation regulating genes *dmpI*, *narJ* and *narK*, and one reduction regulating gene *sod*), which could maintain the intracellular redox balance, to test their expression after treatment by Au NCs and Au NPs. *dmpI* gene encodes 4-oxalocrotonate tautomerase, which involves in the oxidative catabolism of toluene, o-xylene, 3-ethyltoluene, and 1,2,4-trimethylbenzene into corresponding intermediates in the citric acid cycle, producing ROS as byproduct [62]. *narJ* and *narK* genes are important participants in the respiratory nitrate reductase, transferring electrons from NADH or NADPH to nitrate, assisting the nitrate transport coupled to nitrate reduction [63]. The reduction regulating *sod* gene encodes the intracellular ROS scavenger SOD enzyme, which could inhibit the oxidative metabolism reaction [64,65]. As shown in Fig. 4c–f, all three Au NCs induced significant up-regulation expression of pro-oxidative genes, and significant down-regulation expression of anti-oxidant gene, which are consistent with our previous reports [33,42]. The gene expression data suggest that the internalized Au NCs could cause metabolic imbalance through promotion of pro-oxidative enzymes and suppression of anti-oxidative enzymes, which could result in overall accumulation of intracellular ROS that lead to the bacterial death. In contrast, Au NPs treated groups did not show any appreciable change in the gene expressions, suggesting their poor uptake inside bacteria would lead to minimal disturbance towards the bacterial metabolism process, resulting in weak antimicrobial ability. These size matters are not trivial as many may translate their understanding of eukaryotic cellular endocytosis to the bacterial system. There is no cellular endocytosis mechanism that particles can engage with in these microbes. If there is any observed killing, it is likely to be extracellular originated which would be gravely hampered by external dilution factors by the environment. However, if the same antimicrobial agent is able to enter the cells by merely accommodating to the intrinsic physical pores of the bacterial wall, it greatly increases the intracellular concentration to lethal levels.

4. Conclusion

In conclusion, we have built a library of three different sized ultrasmall Au NCs (Au_{25}, Au_{102}, and Au_{144}) and two larger sized Au NPs (~3 and ~5 nm) protected by the same ligand to study their bacterial killing behaviors. The ultrasmall Au NCs (~1 nm) could be easily and effectively internalized by the bacteria to achieve antimicrobial effect. In contrast, larger sized Au NPs showcased ineffective internalization that resulted in the absence of bacterial killing effects, indicating the key role of size on antimicrobial ability. Once the Au NCs have been internalized, they would work in a unit to show molecule-like instead of size-dependent antimicrobial behavior, possessing the comparable bacterial killing efficacy with an IC_{50} value of ~2.4 μM on the basis of molecular concentration of Au NCs. After internalization, the Au NCs could generate ROS to oxidize bacterial membrane and disturb bacterial normal metabolism, leading to severe bacterial killing effect. Our finding on molecule-like antimicrobial ability of Au NCs is different from the previously reported size-dependent biomedical applications of nanomaterials, indicating the unique biological behaviors of ultrasmall metal NCs which deserves systematic investigation. Our work also

suggests the key role of internalization on the efficacy of biomedical applications of nanomaterials, which would promote the rational design of high-performance theranostic probes according to size control in the future.

CRediT authorship contribution statement

Kaiyuan Zheng: Conceptualization, Methodology, Investigation, Data curation, Writing - original draft. **Magdiel I. Setyawati:** Conceptualization, Writing - review & editing. **David Tai Leong:** Conceptualization, Writing - review & editing, Supervision. **Jianping Xie:** Conceptualization, Writing - review & editing, Supervision.

Declaration of competing interest

There are no conflicts to declare.

Acknowledgements

This work was financially supported by Ministry of Education, Singapore, under Grant R-279-000-580-112 and R-279-000-538-114.

Appendix A. Supplementary data

Supplementary data to this article can be found online at https://doi.org/10.1016/j.bioactmat.2020.09.026.

References

[1] A.E. Nel, L. Mädler, D. Velegol, T. Xia, E.M. Hoek, P. Somasundaran, F. Klaessig, V. Castranova, M. Thompson, Understanding biophysicochemical interactions at the nano–bio interface, Nat. Mater. 8 (2009) 543–557.
[2] A. Verma, F. Stellacci, Effect of surface properties on nanoparticle–cell interactions, Small 6 (2010) 12–21.
[3] A.M. Alkilany, S.E. Lohse, C.J. Murphy, The gold standard: gold nanoparticle libraries to understand the nano–bio interface, Acc. Chem. Res. 46 (2012) 650–661.
[4] C.Y. Tay, M.I. Setyawati, J. Xie, W.J. Parak, D.T. Leong, Back to basics: exploiting the innate physico-chemical characteristics of nanomaterials for biomedical applications, Adv. Funct. Mater. 24 (2014) 5936–5955.
[5] J. Zhu, C. Sevencan, M. Zhang, R.S.A. McCoy, X. Ding, J. Ye, J. Xie, K. Ariga, J. Feng, B.-H. Bay, Increasing potential interacting area of nanomedicine enhances its homotypic cancer targeting efficacy, ACS Nano 14 (2020) 3259–3271.
[6] C. He, Y. Hu, L. Yin, C. Tang, C. Yin, Effects of particle size and surface charge on cellular uptake and biodistribution of polymeric nanoparticles, Biomaterials 31 (2010) 3657–3666.
[7] Y. Pan, S. Neuss, A. Leifert, M. Fischler, F. Wen, U. Simon, G. Schmid, W. Brandau, W. Jahnen-Dechent, Size-dependent cytotoxicity of gold nanoparticles, Small 3 (2007) 1941–1949.
[8] K. Zheng, M.I. Setyawati, D.T. Leong, J. Xie, Antimicrobial silver nanomaterials, Coord. Chem. Rev. 357 (2018) 1–17.
[9] T.L. Moore, L. Rodriguez-Lorenzo, V. Hirsch, S. Balog, D. Urban, C. Jud, B. Rothen-Rutishauser, M. Lattuada, A. Petri-Fink, Nanoparticle colloidal stability in cell culture media and impact on cellular interactions, Chem. Soc. Rev. 44 (2015) 6287–6305.
[10] S.J. Soenen, W.J. Parak, J. Rejman, B. Manshian, (Intra)cellular stability of inorganic nanoparticles: effects on cytotoxicity, particle functionality, and biomedical applications, Chem. Rev. 115 (2015) 2109–2135.
[11] N. Feliu, D. Docter, M. Heine, P. del Pino, S. Ashraf, J. Kolosnjaj-Tabi, P. Macchiarini, P. Nielsen, D. Alloyeau, F. Gazeau, *Invivo* degeneration and the fate of inorganic nanoparticles, Chem. Soc. Rev. 45 (2016) 2440–2457.
[12] R. Jin, C. Zeng, M. Zhou, Y. Chen, Atomically precise colloidal metal nanoclusters and nanoparticles: fundamentals and opportunities, Chem. Rev. 116 (2016) 10346–10413.
[13] P.D. Jadzinsky, G. Calero, C.J. Ackerson, D.A. Bushnell, R.D. Kornberg, Structure of a thiol monolayer-protected gold nanoparticle at 1.1 Å resolution, Science 318 (2007) 430–433.
[14] A. Desireddy, B.E. Conn, J. Guo, B. Yoon, R.N. Barnett, B.M. Monahan, K. Kirschbaum, W.P. Griffith, R.L. Whetten, U. Landman, Ultrastable silver nanoparticles, Nature 501 (2013) 399–402.
[15] M. Zhou, T. Higaki, G. Hu, M.Y. Sfeir, Y. Chen, D.-e. Jiang, R. Jin, Three-orders-of-magnitude variation of carrier lifetimes with crystal phase of gold nanoclusters, Science 364 (2019) 279–282.
[16] I. Chakraborty, T. Pradeep, Atomically precise clusters of noble metals: emerging link between atoms and nanoparticles, Chem. Rev. 117 (2017) 8208–8271.
[17] J. Xie, Y. Zheng, J.Y. Ying, Protein-directed synthesis of highly fluorescent gold nanoclusters, J. Am. Chem. Soc. 131 (2009) 888–889.
[18] S. Knoppe, T. Bürgi, Chirality in thiolate-protected gold clusters, Acc. Chem. Res. 47 (2014) 1318–1326.
[19] S. Yamazoe, K. Koyasu, T. Tsukuda, Nonscalable oxidation catalysis of gold clusters, Acc. Chem. Res. 47 (2013) 816–824.
[20] L. Shang, S. Dong, G.U. Nienhaus, Ultra-small fluorescent metal nanoclusters: synthesis and biological applications, Nano Today 6 (2011) 401–418.
[21] L. Zhang, E. Wang, Metal nanoclusters: new fluorescent probes for sensors and bioimaging, Nano Today 9 (2014) 132–157.
[22] C.M. Aikens, Electronic and geometric structure, optical properties, and excited state behavior in atomically precise thiolate-stabilized noble metal nanoclusters, Acc. Chem. Res. 51 (2018) 3065–3073.
[23] Q. Tang, G. Hu, V. Fung, D.-e. Jiang, Insights into interfaces, stability, electronic properties, and catalytic activities of atomically precise metal nanoclusters from first principles, Acc. Chem. Res. 51 (2018) 2793–2802.
[24] X. Kang, M. Zhu, Tailoring the photoluminescence of atomically precise nanoclusters, Chem. Soc. Rev. 48 (2019) 2422–2457.
[25] S. Choi, R.M. Dickson, J. Yu, Developing luminescent silver nanodots for biological applications, Chem. Soc. Rev. 41 (2012) 1867–1891.
[26] Y. Tao, M. Li, J. Ren, X. Qu, Metal nanoclusters: novel probes for diagnostic and therapeutic applications, Chem. Soc. Rev. 44 (2015) 8636–8663.
[27] H. Zhang, H. Liu, Z. Tian, D. Lu, Y. Yu, S. Cestellos-Blanco, K.K. Sakimoto, P. Yang, Bacteria photosensitized by intracellular gold nanoclusters for solar fuel production, Nat. Nanotechnol. 13 (2018) 900–905.
[28] W. Zhou, X. Gao, D. Liu, X. Chen, Gold nanoparticles for *in vitro* diagnostics, Chem. Rev. 115 (2015) 10575–10636.
[29] B. Du, X. Jiang, A. Das, Q. Zhou, M. Yu, R. Jin, J. Zheng, Glomerular barrier behaves as an atomically precise bandpass filter in a sub-nanometre regime, Nat. Nanotechnol. 12 (2017) 1096–1102.
[30] K. Zheng, J. Xie, Engineering ultrasmall metal nanoclusters as promising theranostic agents, Trends Chem. 2 (2020) 665–679.
[31] X.-R. Song, N. Goswami, H.-H. Yang, J. Xie, Functionalization of metal nanoclusters for biomedical applications, Analyst 141 (2016) 3126–3140.
[32] Z. Luo, K. Zheng, J. Xie, Engineering ultrasmall water-soluble gold and silver nanoclusters for biomedical applications, Chem. Commun. 50 (2014) 5143–5155.
[33] K. Zheng, M.I. Setyawati, D.T. Leong, J. Xie, Antimicrobial gold nanoclusters, ACS Nano 11 (2017) 6904–6910.
[34] Y. Li, J. Zhen, Q. Tian, C. Shen, L. Zhang, K. Yang, L. Shang, One step synthesis of positively charged gold nanoclusters as effective antimicrobial nanoagents against multidrug-resistant bacteria and biofilms, J. Colloid Interface Sci. 569 (2020) 235–243.
[35] H. Yang, R. Cai, Y. Zhang, Y. Chen, B. Gu, Gold nanoclusters as an antibacterial alternative against clostridium difficile, Int. J. Nanomed. 15 (2020) 6401–6408.
[36] T.-K. Chang, T.-M. Cheng, H.-L. Chu, S.-H. Tan, J.-C. Kuo, P.-H. Hsu, C.-Y. Su, H.-M. Chen, C.-M. Lee, T.-R. Kuo, Metabolic mechanism investigation of antibacterial active cysteine-conjugated gold nanoclusters in *Escherichia coli*, ACS Sustain. Chem. Eng. 7 (2019) 15479–15486.
[37] M. Turner, V.B. Golovko, O.P. Vaughan, P. Abdulkin, A. Berenguer-Murcia, M.S. Tikhov, B.F. Johnson, R.M. Lambert, Selective oxidation with dioxygen by gold nanoparticle catalysts derived from 55-atom clusters, Nature 454 (2008) 981–983.
[38] M. Tsoli, H. Kuhn, W. Brandau, H. Esche, G. Schmid, Cellular uptake and toxicity of Au_{55} clusters, Small 1 (2005) 841–844.
[39] Y. Zhang, P. Song, T. Chen, X. Liu, T. Chen, Z. Wu, Y. Wang, J. Xie, W. Xu, Unique size-dependent nanocatalysis revealed at the single atomically precise gold cluster level, Proc. Natl. Acad. Sci. U.S.A. 115 (2018) 10588–10593.
[40] Z. Luo, V. Nachammai, B. Zhang, N. Yan, D.T. Leong, D.-e. Jiang, J. Xie, Toward understanding the growth mechanism: tracing all stable intermediate species from reduction of Au(I)–thiolate complexes to evolution of Au_{25} nanoclusters, J. Am. Chem. Soc. 136 (2014) 10577–10580.
[41] O.A. Wong, C.L. Heinecke, A.R. Simone, R.L. Whetten, C.J. Ackerson, Ligand symmetry-equivalence on thiolate protected gold nanoclusters determined by NMR spectroscopy, Nanoscale 4 (2012) 4099–4102.
[42] K. Zheng, M.I. Setyawati, D.T. Leong, J. Xie, Surface ligand chemistry of gold nanoclusters determines their antimicrobial ability, Chem. Mater. 30 (2018) 2800–2808.
[43] J. Liu, N. Jian, I. Ornelas, A.J. Pattison, T. Lahtinen, K. Salorinne, H. Häkkinen, R.E. Palmer, Exploring the atomic structure of 1.8 nm monolayer-protected gold clusters with aberration-corrected STEM, Ultramicroscopy 176 (2017) 146–150.
[44] S. Eustis, M.A. El-Sayed, Why gold nanoparticles are more precious than pretty gold: noble metal surface plasmon resonance and its enhancement of the radiative and nonradiative properties of nanocrystals of different shapes, Chem. Soc. Rev. 35 (2006) 209–217.
[45] S.K. Ghosh, T. Pal, Interparticle coupling effect on the surface plasmon resonance of gold nanoparticles: from theory to applications, Chem. Rev. 107 (2007) 4797–4862.
[46] F. Bertorelle, I. Russier-Antoine, C. Comby-Zerbino, F. Chirot, P. Dugourd, P.-F.o. Brevet, R. Antoine, Isomeric effect of mercaptobenzoic acids on the synthesis, stability, and optical properties of $Au_{25}(MBA)_{18}$ nanoclusters, ACS Omega 3 (2018) 15635–15642.
[47] Y. Levi-Kalisman, P.D. Jadzinsky, N. Kalisman, H. Tsunoyama, T. Tsukuda, D.A. Bushnell, R.D. Kornberg, Synthesis and characterization of Au_{102}(p-MBA)$_{44}$ nanoparticles, J. Am. Chem. Soc. 133 (2011) 2976–2982.
[48] H. Qian, R. Jin, Controlling nanoparticles with atomic precision: the case of Au_{144}(SCH2CH2Ph)$_{60}$, Nano Lett. 9 (2009) 4083–4087.
[49] J. Kim, D. Lee, Size-controlled interparticle charge transfer between TiO_2 and quantized capacitors, J. Am. Chem. Soc. 129 (2007) 7706–7707.
[50] T. Lahtinen, E. Hulkko, K. Sokołowska, T.-R. Tero, V. Saarnio, J. Lindgren, M. Pettersson, H. Häkkinen, L. Lehtovaara, Covalently linked multimers of gold

nanoclusters Au_{102}(*p*-MBA)$_{44}$ and $Au_{\sim 250}$(*p*-MBA)$_n$, Nanoscale 8 (2016) 18665–18674.
[51] R. Benz, Porin from bacterial and mitochondrial outer membranes, CRC Crit. Rev. Biochem. 19 (1985) 145–190.
[52] M. Zhu, C.M. Aikens, F.J. Hollander, G.C. Schatz, R. Jin, Correlating the crystal structure of a thiol-protected Au_{25} cluster and optical properties, J. Am. Chem. Soc. 130 (2008) 5883–5885.
[53] N. Yan, N. Xia, L. Liao, M. Zhu, F. Jin, R. Jin, Z. Wu, Unraveling the long-pursued Au_{144} structure by X-ray crystallography, Sci. Adv. 4 (2018) eaat7259.
[54] K. Zheng, J. Xie, Composition dependent antimicrobial ability of full-spectrum Au_xAg_{25-x} alloy nanoclusters, ACS Nano 14 (2020) 11533–11541.
[55] X. Ding, F. Peng, J. Zhou, W. Gong, G. Slaven, K.P. Loh, C.T. Lim, D.T. Leong, Defect engineered bioactive transition metals dichalcogenides quantum dots, Nat. Commun. 10 (2019) 41.
[56] B.L. Li, R. Li, H.L. Zou, K. Ariga, N.B. Li, D.T. Leong, Engineered functionalized 2D nanoarchitectures for stimuli-responsive drug delivery, Mater. Horiz. 7 (2020) 455–469.
[57] D. Wu, B.L. Li, Q. Zhao, Q. Liu, D. Wang, B. He, Z. Wei, D.T. Leong, G. Wang, H. Qian, Assembling defined DNA nanostructure with nitrogen-enriched carbon dots for theranostic cancer applications, Small 16 (2020) 1906975.
[58] K. Zheng, M.I. Setyawati, T.-P. Lim, D.T. Leong, J. Xie, Antimicrobial cluster bombs: silver nanoclusters packed with daptomycin, ACS Nano 10 (2016) 7934–7942.
[59] A. Ayala, M.F. Muñoz, S. Argüelles, Lipid peroxidation: production, metabolism, and signaling mechanisms of malondialdehyde and 4-hydroxy-2-nonenal, Oxid. Med. Cell. Longev. 2014 (2014) 360438.
[60] M. Valko, D. Leibfritz, J. Moncol, M.T. Cronin, M. Mazur, J. Telser, Free radicals and antioxidants in normal physiological functions and human disease, Int. J. Biochem. Cell Biol. 39 (2007) 44–84.
[61] K. Apel, H. Hirt, Reactive oxygen species: metabolism, oxidative stress, and signal transduction, Annu. Rev. Plant Biol. 55 (2004) 373–399.
[62] C.P. Whitman, The 4-oxalocrotonate tautomerase family of enzymes: how nature makes new enzymes using a β–α–β structural motif, Arch. Biochem. Biophys. 402 (2002) 1–13.
[63] S. Fuchs, J. Pané-Farré, C. Kohler, M. Hecker, S. Engelmann, Anaerobic gene expression in *Staphylococcus aureus*, J. Bacteriol. 189 (2007) 4275–4289.
[64] J.M. McCord, I. Fridovich, Superoxide dismutase an enzymic function for erythrocuprein (hemocuprein), J. Biol. Chem. 244 (1969) 6049–6055.
[65] J. Fee, Regulation of sod genes in *Escherichia coli*: relevance to superoxide dismutase function, Mol. Microbiol. 5 (1991) 2599–2610.
[66] F. Peng, M.I. Setyawati, J.K. Tee, X. Ding, J. Wang, M.E. Nga, H.K. Ho, D.T. Leong, Nanoparticles promote *in vivo* breast cancer cell intravasation and extravasationby inducing endothelial leakiness, Nat. Nanotechnol. 14 (2019) 279–286.